Published in final edited form as:
*Lab Chip*. 2013 April 21; 13(8): 1644–1648. doi:10.1039/c3lc41415a.

# Microfluidic oscillators with widely tunable periods

**Sung-Jin Kim**[a], **Ryuji Yokokawa**[a,b], and **Shuichi Takayama**[a,c,d,*]

[a]Department of Biomedical Engineering, University of Michigan, Ann Arbor, MI, 48109, USA

[b]Department of Microengineering, Kyoto University, Yoshida-honmachi, Sakyo, Kyoto, 606-8501 JAPAN

[c]Department of Macromolecular Science and Engineering, University of Michigan, Ann Arbor, MI, 48109, USA

[d]Division of Nano-Bio and Chemical Engineering WCU Project, UNIST, Ulsan, Republic of Korea

## Abstract

We present experiments and theory of a constant flow-driven microfluidic oscillator with widely tunable oscillation periods. This oscillator converts two constant input-flows from a syringe pump into an alternating, periodic output-flow with oscillation periods that can be adjusted to between 0.3 s to 4.1 h by tuning an external membrane capacitor. This capacitor allows multiple adjustable periods at a given input flow-rate, thus providing great flexibility in device operation. Also, we show that a sufficiently large external capacitance, relative to the internal capacitance of the microfluidic valve itself, is a critical requirement for oscillation. These widely tunable microfluidic oscillators are envisioned to be broadly useful for the study of biological rhythms, as on-chip timing sources for microfluidic logic circuits, and other applications that require variation in timed flow switching.

## 1. Introduction

Oscillation is not only ubiquitous but also crucial in biological,[1–4] chemical,[5, 6] and electronic[7] systems. For instance, electronic oscillators are widely used to make clock signals for the coordination of circuit functions. Biological oscillators are also prevalent and essential: neurons generate periodic action potentials, and hormonal cells periodically secret biochemicals to alter cell metabolism. Due to the distinctive functions of each biological oscillator, each biological oscillation has remarkably different period, ranging from sub second to a month.[1]

Less developed but intriguing for biochemical applications and fluidic device development are microfluidic oscillators.[8–12] With a function analogous to electronic DC to AC conversion, the output of the microfluidic oscillator can be used as on-chip timing sources for microfluidic logic gates[12–16] and as a periodic, biochemical stimulator for biological samples.[17–21] A major limitation of previously reported microfluidic oscillators, however, is that they have one pre-defined oscillation period for a given flow rate. To adjust oscillation periods, the input flow rates has to be altered and even then the previously reported oscillators operate within a moderate periodic range of a second to few minutes[8,9] or exclusively at very fast periods (< sec).[10–12]

Here, this paper develops a theoretical understanding and performs experimental validation of a novel constant flow-driven microfluidic oscillator, where external capacitors are used to

*To whom correspondence should be addressed. takayama@umich.edu.

enable a broad range of oscillation periods without changing input flow rates (Fig. 1). We show theoretically that arbitrarily long oscillation periods are possible by simply increasing the external capacitance. In contrast, short oscillation periods are limited by the condition where the external capacitance must be larger than that of the internal capacitance of the fluidic valve components. We then experimentally demonstrate the ability to drive an oscillator at different periods that span 4 orders of magnitude by using a combination of different capacitance and flow rates.

## 2. Experimental

### 2.1. Device fabrication and its structure

Device fabrication and experimental setups are explained in our previous study.[9] Each device consists of three layers of poly(dimethylsiloxane) (PDMS): top and bottom slab for channel and valve features, and a thin membrane middle layer (Right panel of Fig. 1A). The height of channels and valves were 75 μm. External membrane capacitors also consist of three layers of PDMS (Left panel of Fig. 1A), and the diameter and the thickness of the external membrane capacitor were varied in the range of 2–11 mm and 10–40 μm, respectively. Two pressure sensors were connected at the inlets to measure the pressures of microfluidic valves' top side, and a syringe pump was used to provide a constant flow. The working solution was deionized water.

### 2.2. Device parameters

The pressure change of a fluidic system is converted to an elastic energy by a mechanical capacitor having a flexible solid layer. The larger the capacitance is, the slower the pressure change is. The capacitances in our oscillator system can be separated into “external” capacitances ($C_e$) and “internal” capacitances ($C_i$); see Fig. 1A and 1B. $C_e$ is determined by the combined effects of connection tubes, pressure sensors, and the tunable membrane-capacitors which are all external to the core oscillator circuits comprised of two inter-connected switching valves (Fig. 1B). On the other hand, $C_i$ arises mainly from the flexibility of the switching valve's membrane.

Difference between the pressure of the valve's bottom actuation chamber ($P_B$, right panel of Fig. 1A) and that of the valve's top-side inlet ($P_T$) determines open and close state of the valve. Specifically, the valve-open condition is given by

$$P_T - P_B > P_{th-open}, \quad (1)$$

where $P_{th\text{-}open}$ is open threshold pressure. The valve-close condition is given by

$$P_T - P_B < P_{th-open}, \quad (2)$$

where $P_{th\text{-}close}$ is close threshold pressure. The meaning of equations 1 and 2 are as follows: Once the valve is open, it is not closed until $P_T - P_B < P_{th\text{-}close}$ is satisfied. Also, once the valve is closed, it does not open until $P_T - P_B > P_{th\text{-}open}$.

$P_{th\text{-}open}$ is defined as the difference between $P_T$ and $P_B$ as a valve opens. This $P_{th\text{-}open}$ is also approximately the difference between valve 1 and 2's $P_T$ ($P_{T1}$ and $P_{T2}$) as each valve opens because the fluidic resistance $R_4$ (Fig. 1C) is one order of magnitude higher than the fluidic resistances $R_2$ and $R_3$ (Supplementary Fig. S1). As a result, the fluidic resistance condition enables the following approximation:

$$P_{B1} \approx P_{T2} \text{ when valve 2 opens} \quad (3)$$

$$P_{B2} \approx P_{T1} \text{ when valve 1 opens} \quad (4)$$

This approximation is practically useful as it eliminated the needs to measure the pressures of the bottom actuation chamber ($P_{B1}$ and $P_{B2}$). In our oscillators, we measured a $P_{th\text{-}close}$ of − 1 ± 0.2 kPa.[22] Commercial software (PLECS, Plexim GmbH, Switzerland) was used for the numerical simulation of the microfluidic oscillator. For the simulation, we used theoretical value of $C_i$ and measured values of $C_e$, $P_{th\text{-}close}$, and $P_{th\text{-}close}$.

## 3. Results and Discussion

### 3.1. Influence of $C_e$ plus $C_i$ on oscillation period

Understanding the effect of capacitances in the context of valve operation is key to designing functional period-adjustable oscillators. The minimalistic oscillator has two microfluidic valves connected to each other, where the output of one valve's top inlet connects to the bottom actuation chamber of the other and vice versa. This inter-connectedness leads to the two valves alternating with each other in terms of when each valve is open or closed.

This process is illustrated in Fig. 2, where a red and a clear solution are infused at a constant flow rate. When valve 2 is open (Top panel of Fig. 2A), the red solution flows through the bottom actuation chamber of valve 1, closing it off, then exiting through the outlet. During this process, $P_{B1}$ as well as the interconnected $P_{T2}$ decreases (equation 3). On the other hand, because valve 1 is closed $P_{T1}$ increases as the clear solution continues to be infused but with no place to exit. Thus, $P_{T1} - P_{B1}$ gradually increases and when $P_{T1} - P_{B1}$ eventually surpasses $P_{th\text{-}open}$ (equation 1), valve 1 opens (Bottom panel of Fig. 2A). As valve 1 opens, the clear solution flows through the bottom actuation chamber of valve 2, closing it off then exiting through the outlet (equation 2). Now, because valve 2 is closed, $P_{T2}$ increases as the red solution continues to be infused but with no place to exit. This process cycles repeatedly resulting in an oscillatory output.

The oscillatory outflow of fluids is accompanied by repeated accumulation and release of $P_{T1}$ and $P_{T2}$ (Figs. 2B and 2C). The accumulation-rate of the closed valve's $P_T$ ($dP_T/dt$) is approximated to be $Q_i/(C_e + C_i)$, where $Q_i$ is inflow rate. Thus as illustrated in Fig. 2B, the duration of a closed-valve state is expressed as

$$(C_e + C_i)\, P_{th-open}/Q_i \quad (5)$$

The oscillation period of a symmetric two valve system is twice this single valve closure duration.

### 3.2. Limits of $C_e$, $C_i$, and $Q_i$ where oscillation is achieved

While equation 5 provides a useful guide for estimating oscillation periods, it only provides a partial picture of oscillator function as not all values of $C_e$, $C_i$, and $Q_i$ support oscillation. Let us first look at how the pressures $P_{T1}$ and $P_{B1}$ of valve 1 changes over time when $C_e > C_i$. Under this condition, $P_{B1}$ becomes sufficiently high upon opening of valve 2; see the second white region of Fig. 3A. As a result, valve 1 can be shut off ($P_{T1} - P_{B1} < P_{th\text{-}close}$). On the other hand, when $C_e$ is ~ $C_i$ or < $C_i$, flow-change created by the opening of valve 2 is buffered by the relatively large internal capacitance leading to insufficient increases in $P_{B1}$ (Gray region of Fig. 3B), and no valve 1 closure. As a result, both valves stay open resulting in a non-oscillatory outflow.

Computational predictions, along with a few experimental examples, of what values of $C_e$, $C_i$, and $Q_i$ support oscillation are summarized in Fig. 4. In our experiment, the valve opening threshold pressures were measured to be between 9 and 40 kPa depending on the valve type. Importantly, when we used large valves having deep trenches (~ 2 mm) to make $C_i$ (Fig. S2) constantly larger than $C_e$, we eliminated oscillations (unfilled circles of Fig. 4).

The critical values of $C_e/C_i$ are in the range of 0.5–11 for the range of capacitances and $Q_i$'s noted. Interestingly, the critical line shifted up as $Q_i$ increased (Fig. 4). That is, for a given $C_i$, the critical value of $C_e$ required for oscillation increases with increasing $Q_i$. Thus, to realize oscillations over a wide range of $Q_i$, an important condition is that $C_e/C_i >> 1$ be maintained. There are two important take away messages: (i) very fast oscillation is possible through small $C_i+C_e$ but under the condition of $C_e/C_i >> 1$. The result implies that, to achieve extremely fast oscillations, connection tubes and syringes as well as other connected components should be rigid to have small $C_e$; furthermore, the membrane of the device should be even more rigid or have less $C_i$. (ii) Extremely slow oscillation is enabled by large $C_e$, not by large $C_i$. It should be noted that the change of $C_e$ does not alter the maximum outflow rate or other operational conditions with respect to $P_{th\text{-}open}$ and fluidic resistances. In other words, the change of $C_e$ should only affect oscillation period. Thus adjusting oscillation periods using an external capacitor is not only convenient but is a great advantage in the design and operation of oscillators.

$P_{th\text{-}open}$ and $Q_i$ can also be adjusted to change oscillation periods (see equation 5). However, altering $P_{th\text{-}open}$ affects outflow rate and other device operation parameters as well. For example, a higher $P_{th\text{-}open}$ (Fig. 2B) would result not only in slow oscillation periods but higher maximum flow rates as well. A low $P_{th\text{-}open}$ should theoretically lead to faster oscillation periods at lower maximum flow rates. Higher $Q_i$ can also give faster oscillations accompanied by higher outflow rates. However, when $Q_i$ surpasses a critical value, oscillation stops because the oscillator cannot respond to pressure changes fast enough.[22] Lower $Q_i$ will lead to slow oscillations with no lower limits.

### 3.3. Widely tunable oscillation period

With theoretical predictions in hand, we experimentally tested how changing $C_e$, through external membrane capacitors, would alter oscillation behavior. External membrane capacitors with different radius ($r$) and the thickness ($h$) of the external membrane are readily prepared. Because capacitance scales as $r^6/h^3$ (ref. 23), small changes in $r$ and $h$ can drastically alter capacitance. Figure 5A shows that, through tuning external membrane capacitors, the oscillation period of the same base oscillator circuit can span more than 4 orders of magnitude, from 0.3 s to 4.1 h. Compared to previous oscillators[8–12] that have < 10 times difference between the maximum and minimum oscillation periods, the current scheme provides at least a $10^3$ times wider range. This range covers the period of the many biological oscillations such as neuronal (~ms to ~s), cardiac (~s), and hormonal oscillations (~min to ~hr).[1] Also, our scheme allows multiple adjustable periods at a given input flow-rate whereas previous oscillators have only one period at a given input. Thus, the use of external membrane capacitors provide great flexibility for oscillator operation, expanding their usefulness as an on-chip timing source for microfluidic logic gates[12–16] and as a periodic, biochemical stimulator for biological samples.[17–21]

The inset of Fig. 5A shows that the effective external capacitance decreases at high $Q_i$. This is because the membrane of the external capacitor becomes stiffer as the membrane deflects more at the high $Q_i$'s. The moment at which a valve opens is that moment at which the valve's top-side inlet pressure is at a maximum value ($P_{T\text{-}max}$) (defined in Fig. 2B) and accordingly the moment at which the outflow rate is also at a maximum ($Q_{o\text{-}max}$) (defined in

Fig. 2C). Thus, Fig. 5B simultaneously presents $P_{T\text{-}max}$ and $Q_{o\text{-}max}$ with respect to $Q_i$. Note that although some of the oscillators are not identical, $P_{T\text{-}max}$ (or $Q_{o\text{-}max}$) values are very similar regardless of different $C_e$ because they are the same oscillator type.

## Conclusions

We have explored the role of valve intrinsic and extrinsic capacitance in determining whether a two-valve fluidic circuit will produce oscillatory outflows or not. We found that the use of a sufficiently large external capacitance, relative to the non-negligible intrinsic valve capacitance was critical for oscillation to be supported. Furthermore, within this constraint, we showed that for a given input flow rate, larger external capacitors would lead to slower oscillation periods with minimal effects on the maximum outflow rates. Since external capacitors can be easily exchanged, this provides a practical way for a single base oscillator circuit that is being operated at a constant input flow rate to generate outflows with a wide range of oscillation periods. Although we only showed oscillation periods of up to 4.1 h for the specific base oscillator circuit described, the oscillation period can be further increased by using larger external membrane capacitors or slower inflow rates. Because of the requirement for external capacitance to be larger than the internal valve capacitance, however, obtaining oscillation periods significantly shorter than the demonstrated 0.3 s will require redesign of the valve components.

## Supplementary Material

Refer to Web version on PubMed Central for supplementary material.

## Acknowledgments

This work was supported by the NIH (GM096040-01 & HL084370-05) and Institutional Program for Young Researcher Overseas Visits, Japan Society for the Promotion of Science (JSPS). Devices were partially fabricated in the Lurie Nanofabrication Facility, a member of the National Nanotechnology Infrastructure Network, which is supported by the National Science Foundation.

## References

1. Goldbeter A. Curr. Biol. 2008; 18:R751–R753. [PubMed: 18786378]
2. Yan A, Xu G, Yang Z-B. Proc. Natl. Acad. Sci. USA. 2009; 106:22002–22007. [PubMed: 19955439]
3. Mather W, Bennett M, Hasty J, Tsimring L. Phys. Rev. Lett. 2009; 102:068105. [PubMed: 19257639]
4. Ullner E, Zaikin A, Volkov E, García-Ojalvo J. Phys. Rev. Lett. 2007; 99:148103. [PubMed: 17930726]
5. Noyes RM, Field RJ. Annu. Rev. Phys. Chem. 1974; 25:95–119.
6. Taylor AF, Tinsley MR, Wang F, Huang Z, Showalter K. Science. 2009; 323:614–617. [PubMed: 19179525]
7. Westra, JR.; Verhoeven, CJM.; van Roermund, AHM. Oscillators and oscillator systems: classification, analysis and synthesis. Kluwer Academic Publishers; Boston: 2000. Ch. 2–3
8. Mosadegh B, Kuo C-H, Tung Y-C, S Torisawa Y, Bersano-Begey T, Tavana H, Takayama S. Nature Phys. 2010; 6:433–437. [PubMed: 20526435]
9. Kim S-J, Yokokawa R, Lesher-Perez SC, Takayama S. Anal. Chem. 2012; 84:1152–1156. [PubMed: 22206453]
10. Xia HM, Wang ZP, Fan W, Wijaya A, Wang W, Wang ZF. Lab Chip. 2012; 12:60–64. [PubMed: 22048176]
11. Nguyen TV, Duncan PN, Ahrar S, Hui EE. Lab Chip. 2012; 12:3991–3994. [PubMed: 22968472]
12. Devaraju NS, Unger MA. Lab Chip. 2012; 12:4809–4815. [PubMed: 23000861]

13. Grover WH, Ivester RHC, Jensen EC, Mathies R. Lab Chip. 2006; 6:623–631. [PubMed: 16652177]
14. Jensen EC, Grover WH, Mathies R. J Microelectromech. Syst. 2007; 16:1378–1385.
15. Rhee M, Burns MA. Lab Chip. 2009; 9:3131–3143. [PubMed: 19823730]
16. Weaver J, Melin J, Stark D, Quake SR, Horowitz M. Nature Phys. 2010; 6:218–223.
17. Jovic A, Howell B, Takayama S. Microfluid. Nanofluid. 2009; 6:717–729.
18. Bennett MR, Pang WL, Ostroff N. a, Baumgartner BL, Nayak S, Tsimring LS, Hasty J. Nature. 2008; 454:1119–1122. [PubMed: 18668041]
19. Chronis N, Zimmer M, Bargmann CI. Nat. Methods. 2007; 4:727–731. [PubMed: 17704783]
20. Lucchetta EM, Lee JH, Fu LA, Patel NH, Ismagilov RF. Nature. 2005; 434:1134–1138. [PubMed: 15858575]
21. Jovic A, Howell B, Cote M, Wade SM, Mehta K, Miyawaki A, Neubig RR, Linderman JJ, Takayama S. PLoS Comput. Biol. 2010; 6:e1001040. [PubMed: 21203481]
22. Kim S-J, Yokokawa R, Takayama S. Appl. Phys. Lett. 2012; 101:234107. [PubMed: 23284181]
23. Kovacs, GTA. Micromachined transducers sourcebooks. McGraw-Hill; Singapore: 2000. p. 794

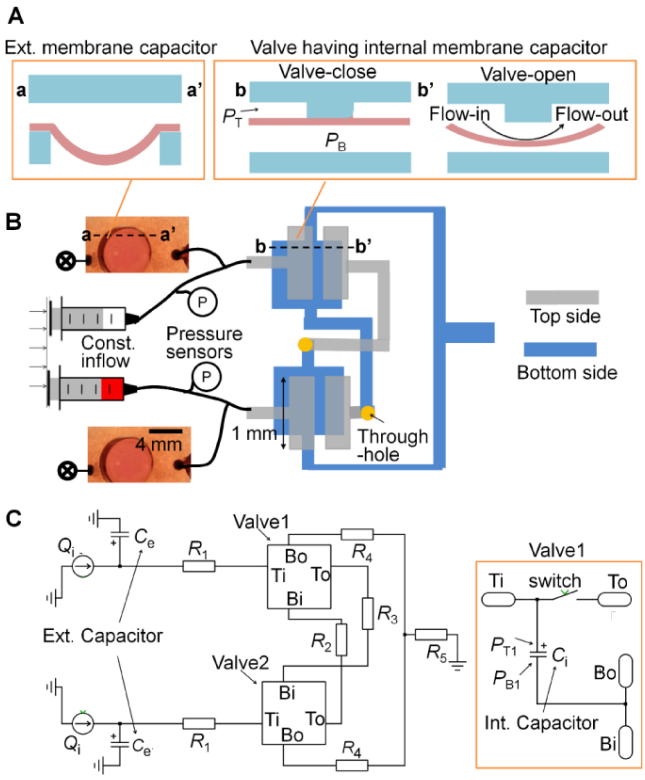


**Fig. 1.**

Microfluidic oscillator with a wide range of period tunability. (A) An external membrane capacitor and a microfluidic valve having an internal membrane capacitor. The valve has a top-side, a bottom actuation chamber, and a membrane. $P_T$ and $P_B$ are pressures at the valve's top-side inlet and bottom actuation chamber, respectively. (B) Schematic of the oscillator system consisting of two valves. It illustrates the three dimensional structure of the system and shows how the two valves are connected to each other. As illustrated in (A), the system has external and internal capacitances ($C_e$ and $C_i$). A syringe pump provides a constant inflow rate, $Q_i$. (C) Circuit diagram of the microfluidic oscillator. The diagram depicts the connection of the valve's top inlet (Ti), top outlet (To), bottom inlet (Bi), and bottom outlet (Bo). Fluidic resistances ($R_1$ to $R_5$) are $5.94\times10^{11}$, $1.38\times10^{12}$, $1.62\times10^{12}$, $2.44\times10^{13}$, $2.27\times10^{11}$ N s m$^{-5}$, respectively.

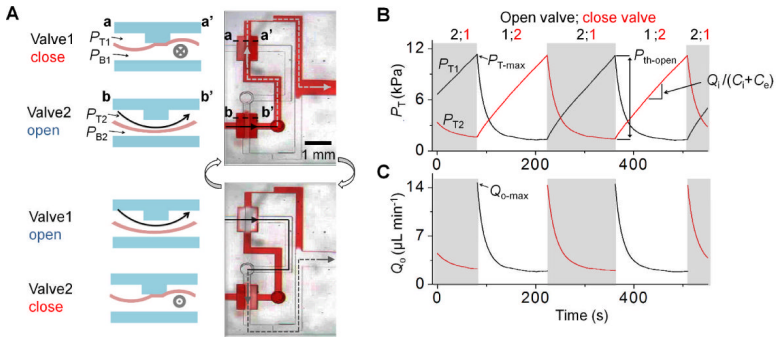


**Fig. 2.**

The two valve self-switching mechanism of the oscillator. (A) Alternating opening and closing of the two valves. Arrows having solid black and dotted gray lines depict the flow directions in the top and the bottom layer of the device, respectively. Note that open and close state of each valve is opposite for oscillation. (B) Measured representative pressure profiles of the two valves' top-side inlets ($P_T$) in the oscillator. (C) Corresponding outflow rate ($Q_o$). In (B) and (C), gray region is valve 2-open and 1-close, and the white region is the opposite.

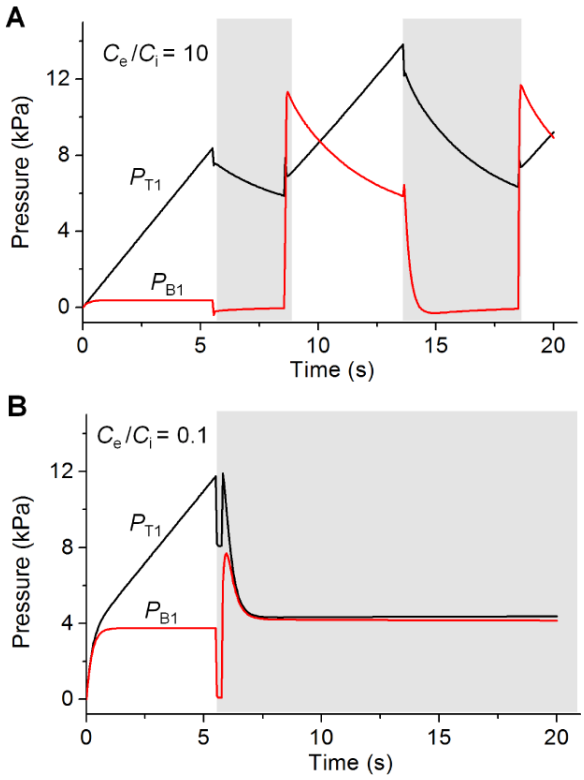


**Fig. 3.**

Pressure profiles of valve 1. Results are from computational simulations. $C_e$+$C_i$ is constant at $10.1\times10^{-13}$ $m^5$/N. $C_e/C_i$ is 10 in (A), which shows oscillations; and 0.1 in (B),which does not oscillate. Gray region is valve 1-open state. $Q_i$ and $P_{th\text{-}open}$ are 10 μL/min and 8 kPa, respectively.

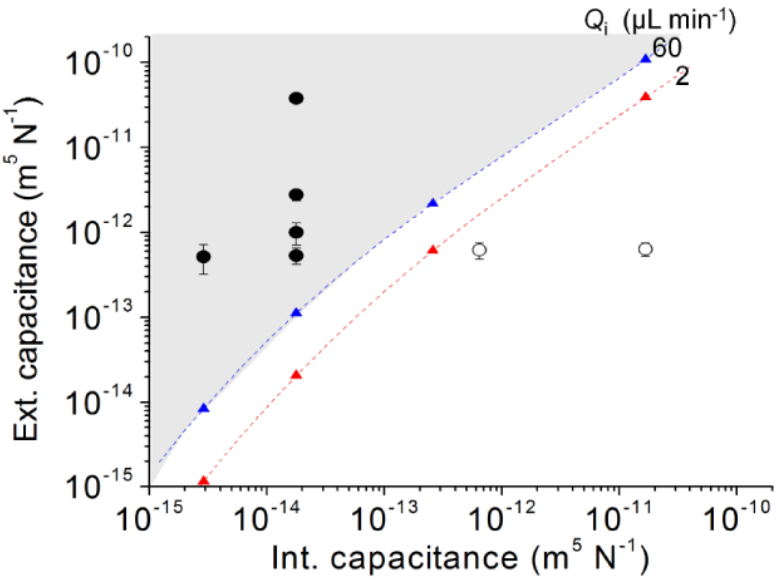


**Fig. 4.**

Computational predictions of what $C_e$ and $C_i$ values will support oscillations for two different values of $Q_i$. Filled circles (•) are experimentally confirmed points within this graph where oscillations are observed, whereas unfilled circles (◦) are experimentally confirmed points where oscillations are not observed. Critical points (▲) and lines are obtained by simulation and cubic polynomial curve fitting, respectively. Thus, the gray region represents the theoretical oscillation region. At the critical points, $C_e/C_i$ values are in the range of 0.5–11 for the given conditions.

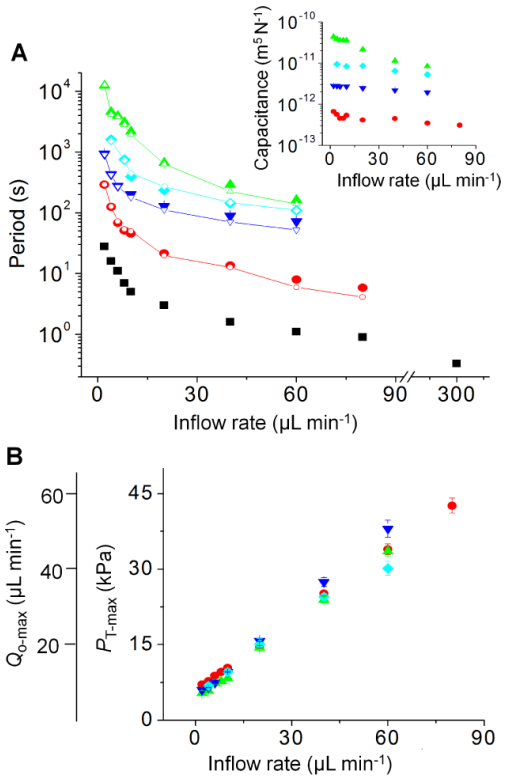


**Fig. 5.**

Widely tunable oscillation periods. Filled and unfilled points are the experimental and simulation results, respectively, and $C_i$ is $1.8\times10^{-14}$ $m^5$ $N^{-1}$. (A) The oscillation period for the same base oscillator circuit can be widely tuned by use of different external capacitors. The actual $C_e$ values of the capacitors that result in each oscillation period are shown in the inset. Note that the same capacitor gives slightly different effective capacitance values depending on inflow rate. (B) Different inflow rates also change maximum pressures ($P_{T\text{-}max}$) and maximum outflow rates ($Q_{o\text{-}max}$). Note that these values do not depend much on capacitor values.